J|A|C|S ARTICLES

Published on Web 05/22/2009

Catalytic Reactivity of a *Meso*-N-Substituted Corrole and Evidence for a High-Valent Iron−Oxo Species

Amanda J. McGown,[†] William D. Kerber,[†] Hiroshi Fujii,[‡] and David P. Goldberg*,[†]

Department of Chemistry, Johns Hopkins University, 3400 North Charles Street, Baltimore Maryland, 21218, and Institute for Molecular Science and Okazaki Institute for Integrative Bioscience, National Institutes of Natural Sciences, Myodaiji, Okazaki 444-8787, Japan

Received November 24, 2008; E-mail: dpg@jhu.edu

Abstract: It is shown that an iron(III) *meso*-N-substituted corrole (TBP_8Cz)Fe^{III} (**1**) (TBP_8Cz = octakis(4-*tert*-butylphenyl)corrolazinato), is a potent catalyst for the oxidation of alkenes in the presence of pentaflouroiodosylbenzene (C_6F_5IO) as oxidant. In the case of cyclohexene, complex **1** performs on a par with one of the best porphyrin catalysts ($(TPPF_{20})FeCl$), exhibiting rapid turnover and a high selectivity for epoxide ($CzFe^{III}$/C_6F_5IO/cyclohexene (1:100:1000) in CH_2Cl_2/CH_3OH (3:1 v:v) gives 33 turnovers of epoxide in <2 min). Reaction rates for **1** are greatly enhanced compared to other Fe or Mn corroles under similar catalytic conditions, consistent with an increase in the electrophilicity of a high-valent iron−oxo intermediate induced by *meso*-N substitution. Reaction of dark-green **1** (λ_{max} = 440, 611, 747 nm) under single-turnover-like conditions at −78 °C leads to the formation of a new dark-brown species (**2**) (λ_{max} = 396, 732, 843 nm). The Fe^{III} complex **1** is restored upon the addition of 2 equiv of ferrocene to **2**, or by the addition of 1 equiv of PPh_3, which concomitantly yields $OPPh_3$. In addition, complex **2** reacts with excess cyclohexene at −42 °C to give **1**. Complex **2** was also characterized by EPR spectroscopy, and all of the data are consistent with **2** being an antiferromagnetically coupled iron(IV)-oxo π-cation-radical complex. Rapid-mixing stopped-flow UV−vis studies show that the low-temperature complex **2** is generated as a short-lived intermediate at room temperature.

Introduction

Much effort has gone into developing heme- and nonheme-based iron complexes as catalysts for a range of oxidation reactions, and as models for related iron-containing enzymes. High-valent iron−oxo ($(L_n)Fe{=}O$) species are proposed to play critical roles in many of these catalytic systems. However, the direct spectroscopic identification or isolation of Fe═O species in both synthetic and biologically relevant catalytic systems has remained a challenging problem because of their inherent instability. For iron porphyrins, high-valent iron−oxo species have been synthesized by reacting a reduced iron porphyrin precursor, typically an iron(III) complex, with a sacrificial oxidant such as PhIO, mCPBA or H_2O_2.[1−3] The product formed has either been oxidized by one electron to give an iron(IV)−oxo complex, or by two electrons to give an iron(IV)−oxo porphyrin-π-cation-radical (the "Compound I" intermediate in heme enzymes). Formally the latter species can be alternatively described as an iron(V)−oxo complex. Extensive investigations have focused on determining the factors that control the formation of these iron−oxo porphyrins, and it is clear from these efforts that many factors such as solvent, temperature and the identity of the oxidant exert a strong influence over what type, if any, of an iron−oxo complex is formed (e.g., (porph)Fe^{IV}(O) versus (porph$^{+\bullet}$)Fe^{IV}(O)).[1−3]

Our approach in this area has been to modify the core of the porphyrin nucleus in a fundamental way so as to stabilize high-valent species, including high-valent metal-oxo complexes. We have focused our efforts on the ring-contraction of tetraazaporphyrins to give *meso*-N-substituted triazacorroles ("corrolazines," (Cz)).[4−6] Metallocorroles, as a general class, have come under intensive investigations worldwide over the past several years.[7−15] These compounds are known to stabilize formally high-valent metal ions, and this stabilization in part comes from

[†] Johns Hopkins University.
[‡] National Institutes of Natural Sciences.

(1) McLain, J. L.; Lee, J.; Groves, J. T. Biomimetic Oxygenations Related to Cytochrome P450: Metal-Oxo and Metal-Peroxo Intermediates. In *Biomimetic Oxidations Catalyzed by Transition Metal Complexes*; Meunier, B., Ed.; Imperial College Press: Cambridge, 2000; Chapter 3, pp 91−169.
(2) Sheldon, R. A. *Metalloporphyrins in Catalytic Oxidations*; Marcel Dekker: New York, 1994.
(3) Nam, W. *Acc. Chem. Res.* **2007**, *40*, 522–531.
(4) Goldberg, D. P. *Acc. Chem. Res.* **2007**, *40*, 626–634.
(5) Gryko, D. T.; Fox, J. P.; Goldberg, D. P. *J. Porphyrins Phthalocyanines* **2004**, *8*, 1091–1105.
(6) Kerber, W. D.; Goldberg, D. P. *J. Inorg. Biochem.* **2006**, *100*, 838–857.
(7) Aviv, I.; Gross, Z. *Chem. Commun.* **2007**, 1987–99.
(8) Bröring, M.; Hell, C.; Steiner, M.; Brandt, C. D. *Z. Anorg. All. Chem.* **2007**, *633*, 1082–1086.
(9) Czernuszewicz, R. S.; Mody, V.; Zareba, A. A.; Zaczek, M. B.; Gałezowski, M.; Sashuk, V.; Grela, K.; Gryko, D. T. *Inorg. Chem.* **2007**, *46*, 5616–5624.
(10) Gross, Z. *J. Biol. Inorg. Chem.* **2001**, *6*, 733–738.
(11) Gross, Z.; Gray, H. B. *Adv. Synth. Catal.* **2004**, *346*, 165–170.
(12) Guilard, R.; Barbe, J. M.; Stern, C.; Kadish, K. M. In *The Porphyrin Handbook*, Kadish, K. M., Smith, K. M., Guilard, R., Eds.; Elsevier: San Diego, 2003; Vol. 18, pp 303−349.
(13) Paolesse, R.; Nardis, S.; Sagone, F.; Khoury, R. G. *J. Org. Chem.* **2001**, *66*, 550–556.
(14) Walker, F. A. *Inorg. Chem.* **2003**, *42*, 4526–4544.
(15) Paolesse, R. *Synlett.* **2008**, 2215–2230.

 10.1021/ja809183z CCC: $40.75

Chart 1

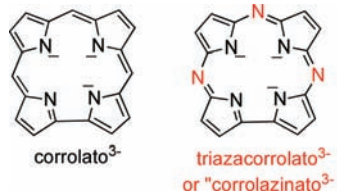

the 3^- charge of the fully deprotonated macrocycle (Chart 1), as compared to the 2^- charge of a deprotonated porphyrin ligand. Surprisingly, there is still only limited information available on the catalytic activity of iron corroles, and even less is known about (corrole)Fe=O species.[16] Only recently has transient absorption data suggested the presence of a high-valent iron−oxo corrole.[17]

Previously the iron(III) corrolazine (TBP_8Cz)Fe^{III} (**1**) (TBP_8Cz = octakis(4-tert-butylphenyl)corrolazinato) was prepared via the general strategy shown in Scheme 1, where an octa-aryl substituted tetraazaporphyrin was ring-contracted to give the metal-free corrolazine ligand TBP_8CzH_3, which was then metalated to give the iron(III) complex **1**.[18] This complex was shown to be an efficient catalyst for the selective oxidation of a variety of thioether substrates with H_2O_2 as the sacrificial oxidant. For example, PhSMe was quantitatively converted to PhS(O)Me (98% yield, 330 turnovers) in 1 min at 23 °C with **1** as catalyst and H_2O_2(aq) added as oxidant (1.1:1.0:0.003 oxidant/substrate/**1** molar ratio).[18] In the absence of a thioether substrate, it was found that **1** was a highly efficient catalyst for the disproportionation of H_2O_2.

The former catalytic behavior of **1** + H_2O_2 was consistent with the intermediacy of a high-valent iron−oxo complex. We expected **1**/H_2O_2 would exhibit other catalytic activity typical of reactive high-valent iron−oxo species, such as the catalytic epoxidation of alkene substrates. However, **1**/H_2O_2 did not catalyze the epoxidation of cyclooctene, a relatively reactive alkene substrate. We also spectroscopically characterized the **1**/H_2O_2/PhSMe reaction mixtures in the hope of observing the formation of a high-valent iron−oxo species. UV−visible spectral analysis of **1**/H_2O_2/thioether reaction mixtures at both room temperature and −78 °C revealed no change in the spectrum of the starting material **1**. In addition, catalytic reaction mixtures

Scheme 1

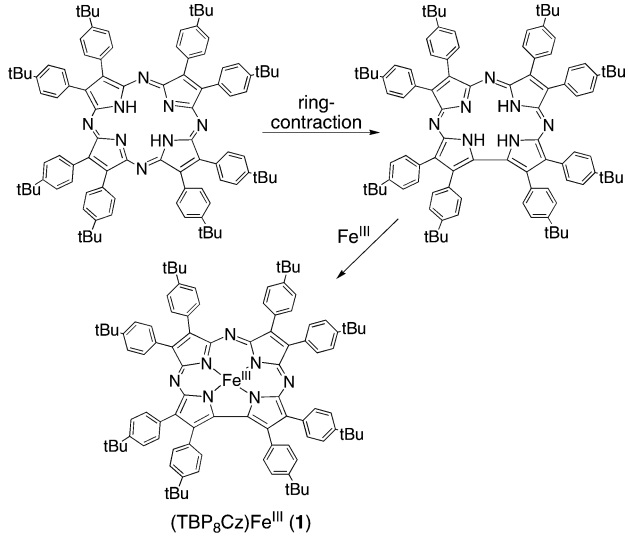

Scheme 2

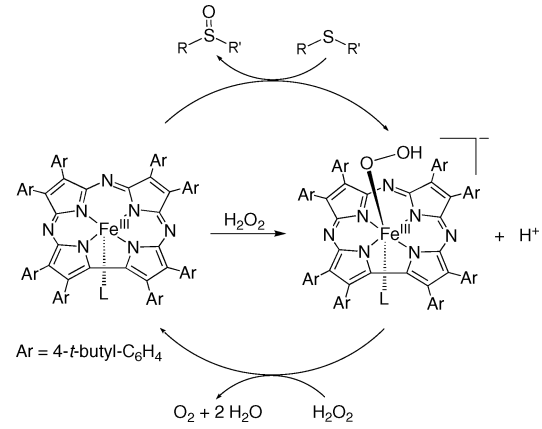

frozen at different time points and analyzed by EPR spectroscopy showed only EPR signals arising from the starting Fe^{III} complex.

The failure of **1**/H_2O_2 to catalyze the epoxidation of alkenes, and the lack of any spectral signature indicating an oxidation state change for the Fe^{III} starting material argued strongly against the generation of a high-valent iron−oxo intermediate. As a final test, we added $H_2{}^{18}O$ to catalytic reaction mixtures with PhSMe as substrate. High-valent iron−oxo porphyrins are known to undergo exchange at the terminal oxo position with $H_2{}^{18}O$, leading to the incorporation of ^{18}O into oxidation products,[19] and we have shown that the Mn^V-oxo corrolazine (TBP_8Cz)Mn^V(O) undergoes facile ^{18}O incorporation upon exposure to $H_2{}^{18}O$.[20,21] There was no ^{18}O incorporation into the PhS(O)Me produced via **1**/H_2O_2/$H_2{}^{18}O$, providing further proof for the absence of a high-valent iron−oxo intermediate in this reaction.

A mechanism for the H_2O_2-dependent oxidations was proposed, and is shown in Scheme 2. The key step is formation of an electrophilic Fe^{III}−OOH species, which then reacts directly with substrate (RSR′ or H_2O_2). The reaction of the metal-(hydro)peroxy intermediate with substrate and/or oxidant is apparently facile, preventing this species from proceeding on to give a high-valent iron−oxo complex. In addition, the same mechanism, with the same metal-hydroperoxide intermediate, was proposed for sulfoxidation and H_2O_2 disproportionation catalyzed by a Mn corrole/albumin conjugate.[22]

In this study we have used iodosylarenes in place of H_2O_2 as the sacrificial oxidant in combination with **1** as catalyst. In contrast to the H_2O_2 reactions, **1** is a potent catalyst for alkene oxidations with ArIO as oxidant. Complex **1** exhibits dramati-

(16) (a) Mahammed, A.; Gross, Z. *Angew. Chem., Int. Ed.* **2006**, *45*, 6544–6547. (b) Grodkowski, J.; Neta, P.; Fujita, E.; Mahammed, A.; Simkhovich, L.; Gross, Z. *J. Phys. Chem. A* **2002**, *106*, 4772–4778. (c) Simkhovich, L.; Gross, Z. *Tetrahedron Lett.* **2001**, *42*, 8089–8092. (d) Simkhovich, L.; Mahammed, A.; Goldberg, I.; Gross, Z. *Chem.−Eur. J.* **2001**, *7*, 1041–1055.
(17) Harischandra, D. N.; Zhang, R.; Newcomb, M. *J. Am. Chem. Soc.* **2005**, *127*, 13776–13777.
(18) Kerber, W. D.; Ramdhanie, B.; Goldberg, D. P. *Angew. Chem., Int. Ed.* **2007**, *46*, 3718–3721.
(19) Bernadou, J.; Fabiano, A.-S.; Robert, A.; Meunier, B. *J. Am. Chem. Soc.* **1994**, *116*, 9375–9376.
(20) Mandimutsira, B. S.; Ramdhanie, B.; Todd, R. C.; Wang, H. L.; Zareba, A. A.; Czernuszewicz, R. S.; Goldberg, D. P. *J. Am. Chem. Soc.* **2002**, *124*, 15170–15171.
(21) Wang, S. H. L.; Mandimutsira, B. S.; Todd, R.; Ramdhanie, B.; Fox, J. P.; Goldberg, D. P. *J. Am. Chem. Soc.* **2004**, *126*, 18–19.
(22) Mahammed, A.; Gross, Z. *J. Am. Chem. Soc.* **2005**, *127*, 2883–2887.

cally different catalytic behavior than Fe or Mn corroles, and remarkably, **1** performs as well as one of the best porphyrin catalysts known ($(F_{20}TPP)FeCl$)[23] ($F_{20}TPP$ = tetrakis(pentafluorophenyl)porphinato) with respect to the epoxidation of cyclohexene under identical reaction conditions. The catalytic behavior of **1** is indicative of a short-lived, high-valent iron−oxo intermediate as the active oxidant, and we have used low-temperature methods to trap and spectroscopically characterize (UV−vis, EPR) the proposed high-valent iron−oxo species, formulated as a Compound I analog, $[(TBP_8Cz^{+\bullet})Fe^{IV}(O)]$ (**2**). The greatly enhanced stability of **2** at low temperature provided us with the opportunity to study its reactivity directly with certain reductants. In addition, rapid-scan, stopped-flow UV−vis studies led to the observation of both the formation and decay of complex **2** at room temperature under catalytic conditions. These data not only helped confirm that the intermediate formed during the room-temperature catalytic reactions is the same as the low-temperature species **2**, but also yielded kinetic information that provided us with further insight into the mechanism of formation and decay of **2**. Apart from the former transient absorption studies,[17] this work provides the first direct spectroscopic evidence for a high-valent iron−oxo corrole.

Experimental Section

General Procedures. All reactions were performed under an atmosphere of argon using dry solvents and standard Schlenk techniques unless otherwise noted. The iron(III) complex $(TBP_8Cz)Fe^{III}$ (TBP = 4-*tert*-butylphenyl) (**1**) was synthesized according to the published method.[18] Pentafluoroiodosylbenzene (PFIB), was synthesized from bis(trifluoroacetoxy)iodo)pentafluorobenzene (Sigma-Aldrich) by modifying a known procedure,[24] as described below. Dichloromethane and methanol were purified via a Pure-Solv solvent purification system from Innovative Technologies, Inc. Deuterated solvents were purchased from Cambridge Isotope Laboratories, Inc. Ethylbenzene, cyclohexene, and decane were purchased from Fluka Chemical Corp. and used as received. All other chemicals were purchased from Sigma-Aldrich and used as received.

Instrumentation. UV−vis spectroscopy was performed on a Varian Cary 50 Bio spectrophotometer, and low-temperature data were collected by using a fiber optic coupler and a Hellma 2 mm quartz immersion probe. Stopped flow data were collected with an Applied Photophysics stopped flow unit (SX.18MV) equipped with a photodiode array spectrophotometer and a 1.0 cm path length optical cell. Electron paramagnetic resonance (EPR) spectra were obtained on a Bruker EMX EPR spectrometer controlled with a Bruker ER 041 X G microwave bridge at 15 K, and equipped with a continuous-flow liquid helium cryostat (ESR900) coupled to a TC503 temperature controller made by Oxford Instruments, Inc. Gas chromatography (GC) was performed on a Shimadzu GC-17A gas chromatograph fitted with a DB-5MS column and interfaced with a Shimadzu QP-5050A mass spectrometer (GC-MS) or an Agilent 6850 gas chromatograph fitted with a DB-5 5% phenylmethyl siloxane capillary column (30 m × 0.32 mm × 0.25 mm) and equipped with a flame-ionization detector. GC-FID response factors for $OPPh_3$ were prepared vs dodecane as an internal standard, and response factors for styrene oxide, phenylacetaldehyde, cyclohexene oxide, 2-cyclohexene-1-ol, 2-cyclohexene-1-one, cyclooctene oxide, 1-phenylethanol, and acetophenone were prepared vs decane as an internal standard. ^{19}F NMR spectra were recorded on a Bruker Avance 300 MHz NMR spectrometer. ^{19}F chemical shifts were set to the known values for C_6F_5I.[25]

EPR Simulations. Theoretical EPR spectral simulations were produced using a computer program that was developed in-house. Simulation parameters: 9.472 GHz, $g_1 = 2.088$ (line width 22.0 G), $g_2 = 2.046$ (line width 29.0 G), $g_3 = 2.024$ (line width 20.0 G), line sharp: Gaussian function, data point: 500, theta division = 500, phi division = 90.

Synthesis of Pentafluoroiodosylbenzene (PFIB). An amount of (bis(trifluoroacetoxy)iodo)pentafluorobenzene (250 mg, 0.481 mmol) was stirred in a saturated solution of sodium bicarbonate (25 mL) open to the air for 24 h. The resulting suspension was filtered to give a white solid, which was washed several times with water. This solid was then dried under vacuum at room temperature in a drying tube over $CaSO_4$ for 12 h, to give PFIB as a yellow powder, 104 mg (70%). *Caution! Heating PFIB under vacuum has been reported to result in an explosion.*[26] The purity of the product was determined by ^{19}F NMR, where the starting material ($C_6F_5I(O_2CCF_3)$) and decomposition product (C_6F_5I) both give distinct ^{19}F NMR spectra. PFIB: ^{19}F NMR (300 MHz, MeOD): −123.2 (2F), −147.9 (1F), −157.7 (2F). $C_6F_5I(O_2CCF_3)$: (300 MHz, MeOD): −75.1 (6F), −121.1 (2F), −144.1 (1F), −156.2 (2F). C_6F_5I: (300 MHz, MeOD): −119.3 (2F), −152.8 (1F), −159.9 (2F). It was noted that the PFIB could be stored up to ∼2 weeks as a solid at −20 °C, at which point decomposition to C_6F_5I was noted.

Catalytic Oxidations. In a typical experiment, a stock solution of catalyst, $(TBP_8Cz)Fe^{III}$ (**1**), was prepared in CD_2Cl_2 (2.83 mM). An amount of this stock solution (125 μL, 0.354 μmol of **1**) was transferred to a 1-dram vial fitted with a septum under Ar, and to this solution was added the alkene or ethylbenzene substrate (0.354 mmol) in 125 μL of CD_2Cl_2 and *n*-decane as internal standard in 125 μL of CD_2Cl_2. While this mixture was being rapidly stirred, a solution of PFIB (35.4 μmol) in 125 μL of CD_3OD was injected to initiate the reaction. A rapid color change from green to brown and then back to green was noted within the first 1−3 s following addition of PFIB. After approximately 10 min the color of **1** faded to a pale yellow, indicating catalyst decomposition. Aliquots of the reaction mixture were directly injected onto the GC for product analysis. The reaction mixture was transferred to an NMR tube and analyzed by ^{19}F NMR spectroscopy, confirming that more than 98% of the PFIB had been converted to C_6F_5I. All yields for **1** or $(F_{20}TPP)FeCl$ reported in Table 1 are based on an average of at least 3 runs. GC-FID conditions for all substrates: An initial oven temperature of 70 °C was held for 3 min and then raised 40 °C/min until a temperature of 100 °C was reached. This temperature was then held for 3.25 min.

Formation of (2) at −78 °C for UV−vis Spectroscopy. In a typical experiment, $(TBP_8Cz)Fe^{III}$ (**1**) (0.336 μmol) was dissolved in 4.5 mL of CH_2Cl_2 in a custom-made Schlenk flask fitted with a quartz immersion probe and attached to a UV−vis spectrophotometer via a fiber optics coupler. The concentration of $(TBP_8Cz)Fe^{III}$ was determined by using the extinction coefficient of the Soret band (λ_{max} 440 nm, (ϵ, 6.30×10^4 M^{-1} cm^{-1})). The solution was cooled

(23) (a) Stephenson, N. A.; Bell, A. T. *J. Am. Chem. Soc.* **2005**, *127*, 8635–8643. (b) Dolphin, D.; Traylor, T. G.; Xie, L. Y. *Acc. Chem. Res.* **1997**, *30*, 251–259. (c) Grinstaff, M. W.; Hill, M. G.; Labinger, J. A.; Gray, H. B. *Science* **1994**, *264*, 1311–1313.
(24) Traylor, T. G.; Miksztal, A. R. *J. Am. Chem. Soc.* **1989**, *111*, 7443–7448.
(25) Lawrenson, I. J. *J. Chem. Soc.* **1965**, 1117–1120.
(26) Collman, J. P. *Chem. Eng. News* **1985**, *63*, 2.
(27) Hessenauer-Ilicheva, N.; Franke, A.; Meyer, D.; Woggon, W.-D.; van Eldik, R. *Chem.−Eur. J.* **2009**, *15*, 2941–2959.
(28) Schardt, B. C.; Hill, C. L. *Inorg. Chem.* **1983**, *22*, 1563–1565.
(29) Traylor, T. G.; Marsters, J. C.; Nakano, T.; Dunlap, B. E. *J. Am. Chem. Soc.* **1985**, *107*, 5537–5539.
(30) Liu, H. Y.; Lai, T. S.; Yeung, L. L.; Chang, C. K. *Org. Lett.* **2003**, *5*, 617–620.
(31) (a) Fox, J. P.; Ramdhanie, B.; Zareba, A. A.; Czernuszewicz, R. S.; Goldberg, D. P. *Inorg. Chem.* **2004**, *43*, 6600–6608. (b) Ramdhanie, B.; Zakharov, L. N.; Rheingold, A. L.; Goldberg, D. P. *Inorg. Chem.* **2002**, *41*, 4105–4107.
(32) Gross, Z.; Simkhovich, L.; Galili, N. *Chem. Commun.* **1999**, 599–600.
(33) Golubkov, G.; Bendix, J.; Gray, H. B.; Mahammed, A.; Goldberg, I.; DiBilio, A. J.; Gross, Z. *Angew. Chem., Int. Ed.* **2001**, *40*, 2132–2134.

Table 1. Catalytic Oxidations by **1**, Fe/Mn Corroles, and Fe Porphyrin

	styrene			cyclohexene						
catalyst[a]	epox	ald	TOF[b]	epox	alc	ket	TOF[b]	time	oxidant	ref
$(TBP_8Cz)Fe^{III}$[c]	**24.0**	**32.3**	**28.2**	**32.7**	**2.0**	**2.0**	**18.4**	**2 min**	**PFIB**	[d]
$(tpfc)Fe^{IV}Cl$[e]	66	21	0.4	–	–	–	–	3.5 h	PhIO	32
$(tpfc)Mn^{III}$[f]	78.0	20.8	0.2	9.3	0.3	1.6	0.02	10−12 h	PhIO	33
$(Br_8tpfc)Mn^{III}$[f]	53.7	45.0	6.6	36.0	32.0	32.0	6.7	15 min	PhIO	33
$(F_8tpfc)Mn^{III}$[f]	56	42	9.8	42	27	25	9.4	10 min	PhIO	30
$(F_{20}TPP)Fe^{III}Cl$[g]	67.9	30.7	49.3	25.7	0.4	4.8	15.5	2 min	PFIB	[d]

[a] All reactions were run at RT with catalyst:oxidant:substrate = 1:100:1000. Product yields (%) were determined based on the oxidant. [b] TOF = Turnover frequency (min^{-1}) = total mol oxidation products/reaction time. [c] [cat] = 0.7 μM in CD_2Cl_2/CD_3OD (3:1). [d] This work. [e] [cat] = 0.36 μM in benzene. [f] [cat] = 1.2 μM, in benzene. [g] [cat] = 0.94 μM in CD_2Cl_2/CD_3OD (3:1).

to −78 °C and 1 equiv of PFIB (0.336 μmol) in 0.250 mL of MeOH was added. The temperature was maintained at −78 °C and the reaction was monitored by UV−vis spectroscopy until complete conversion of **1** into $(TBP_8Cz^{+\bullet})Fe^{IV}(O)$ (**2**) (λ_{max} = 396 nm (ϵ, 4.82×10^4), 732 (ϵ, 5.40×10^3), 843 (ϵ, 3.16×10^3) was observed (∼14 h).

Formation of (2) at −78 °C for EPR Spectroscopy. A typical procedure is as follows: a stock solution of $(TBP_8Cz)Fe^{III}$ in CH_2Cl_2 (2 mM) was prepared. An amount of this stock solution (300 μL, 0.6 μmol) was added to a Wilmad quartz EPR tube (3 mm i.d.) and cooled to −78 °C. An amount of PFIB (0.72 μmol, 1.2 equiv) in 100 μL of CH_3OH was added to the EPR tube and the reaction mixture was bubbled with N_2 or Ar gas for less than 30 s to obtain a homogeneous solution. The reaction mixture was allowed to stand at −78 °C for 10 h, and then the EPR tube was frozen and stored at 77 K until EPR measurements were obtained. Monitoring this reaction at different time-points by EPR showed that the Fe^{III} (intermediate-spin) spectrum for **1** smoothly converted into the spectrum for **2**, with complete loss of **1** noted at the 10 h time-point.

Reaction of (2) with Cp_2Fe. Complex **2** was generated in situ at −78 °C as described above for the UV−vis spectroscopic measurements. After complete formation of **2** was observed by UV−vis, an amount of Cp_2Fe dissolved in CH_2Cl_2 was added. For a typical titration, Cp_2Fe was added in 0.25 equiv increments in 25 μL of CH_2Cl_2 for each addition, up to a total of 4.0 equiv. Monitoring the reaction by UV−vis showed immediate reaction of **2** to give **1** after each addition up to 2.0 equiv, at which point no further change in the spectrum was noted.

Reaction of (2) with PPh_3. An amount of **1** (1.7 mg, 1.2 μmol) was dissolved in 0.600 mL of CH_2Cl_2 and cooled to −78 °C. To this solution was added PFIB (1.2 μmol) in 0.200 mL of CH_3OH. The reaction was stirred for 7 h at −78 °C, during which time the dark-brown color of **2** developed. An amount of PPh_3 (1.33 μmol) in 0.102 mL of CH_2Cl_2 was then added, resulting in the immediate return of the green color characteristic of **1**. After 15 min the reaction was warmed to 23 °C, and dodecane was added as an internal standard before directly analyzing the reaction mixture by GC. The yield of $OPPh_3$ was 104 ± 2% (average of 3 injections) as determined by GC. GC-FID conditions: An initial oven temperature of 140 °C was held for 3 min and then raised 40 °C/min until a temperature of 280 °C was reached. This temperature was then held for 3 min.

Reaction of (2) with Cyclohexene. For product analysis: a stock solution of **1** was prepared in CH_2Cl_2 (18.9 mM). An amount of this stock solution (375 μL, 7.08 μmol of **1**) was transferred to a Schlenk flask and cooled to −78 °C. A solution of PFIB (7.08 μmol) in 125 μL of CH_3OH was then added and the resulting mixture was allowed to stir for 14 h to maximize formation of **2**. Cyclohexene (0.35 mmol, 36 μL, 50 equiv) was added neat and the reaction mixture was stirred for 3 h at −78 °C before warming to room temperature and stirring for an additional 1 h. A solution of decane was added as an internal standard and the reaction mixture was directly injected onto the GC for analysis. Yields reported were an average of 3 runs. UV−vis analysis of the final reaction mixture showed an absorbance value consistent with a 60% recovery of **1**.

Scheme 3

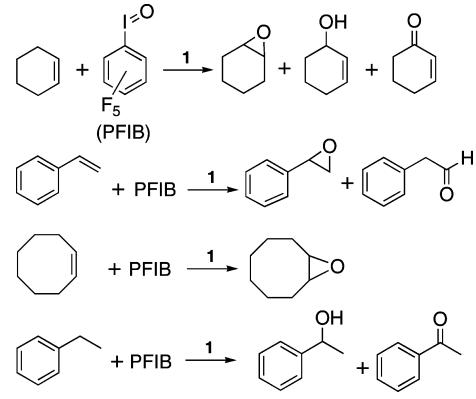

For UV−vis measurements: The formation of **2** was performed at −78 °C and followed by low-temperature UV−vis spectroscopy as described above. After 16 h at −78 °C, the flask was warmed to −42 °C for 15 min and then cyclohexene (0.40 mmol, 41 μL) was added neat. Conversion of **2** to **1** was monitored by UV−vis, and shown to be complete within 30 min.

Stopped-Flow Studies. Stock solutions of **1** (2×10^{-5} M) and PFIB were prepared in 1:1 CH_2Cl_2/CH_3OH and loaded into the stopped-flow driving syringes. In a typical reaction, 100 μL from each syringe was injected into the mixing unit and spectra were collected as rapidly as 2.56 ms, up to a maximum of 2 s. Complete spectra were collected from 300 to 720 nm, and the time dependence of the absorbance at a single wavelength was plotted and fit to an exponential function to give k_{obs}, the pseudo-first-order rate constants. The concentration of PFIB was varied over five different concentrations between $7.03 \times 10^{-4} - 2.74 \times 10^{-3}$ M to determine k^1, the apparent second-order rate constant.

Results and Discussion

Catalytic Oxidations. The results obtained with H_2O_2 as oxidant motivated us to try other O-atom transfer agents, with the goal of generating a bona fide (Cz)Fe(O) species. In previous work we found that reaction of the manganese(III) complex $(TBP_8Cz)Mn^{III}$ with iodosylbenzene (PhIO) led to the synthesis of the manganyl complex $(TBP_8Cz)Mn^{V}(O)$.[20] We speculated that the replacement of H_2O_2 with PhIO, or another iodosylarene, might yield a high-valent iron−oxo species and lead to broader catalytic activity.

Employing pentafluoroiodosylbenzene (PFIB) as oxidant and **1** as catalyst leads to the rapid catalytic oxidation of a variety of substrates (Scheme 3). The catalytic oxidation of styrene with **1**/PFIB/styrene 1:100:1000 equiv in CD_2Cl_2/CD_3OD (3:1 v:v) at 23 °C results in rapid turnover (TOF ≥ 28 min^{-1}) to give styrene oxide (24 TON) and phenylacetaldehyde (32 TON) in less than 2 min (Table 1), the time necessary for injection onto the GC. Control reactions were run with styrene oxide added

as substrate to show that the oxide was not converted to aldehyde under these conditions. With cyclohexene as substrate, rapid turnover also occurs (TOF ≥ 18 min^{-1}), and in this case a striking selectivity for epoxide (33 TON) over other products (alcohol or ketone) is observed. Fast epoxidation of cyclooctene (33 TON) also takes place. Addition of ethylbenzene as substrate leads to oxidation at the benzylic C−H position to give phenylethyl alcohol (2.5 TON) and phenylethyl ketone (6.1 TON). It is clear from these results that the reactivity of **1** + PFIB is dramatically different from that seen for **1** + H_2O_2, and indicates that a more powerful oxidizing agent is being generated. The likely candidate for this stronger oxidant is a bona fide high-valent iron−oxo species.

The unsubstituted PhIO can be used in the former catalytic oxidations, but PFIB was preferred as the oxidant because its consumption, and the concomitant production of C_6F_5I, was readily monitored by ^{19}F NMR spectroscopy. In addition, the stability of PFIB could be checked by ^{19}F NMR, and it was found to have a shelf life of ∼2 weeks when stored as a solid at −20 °C, after which time a significant amount of decay to C_6F_5I was noted. Thus all batches of PFIB were prepared fresh (<2 weeks) prior to use. Although PFIB is only slightly soluble in CH_2Cl_2, it dissolves readily in the mixed solvent system (CH_2Cl_2/CH_3OH) that was employed. Previous workers have noted that PFIB is solvated in alcohol (ROH) solutions to give $C_6F_5I(OH)(OR)$,[27−29] and it is this form that presumably reacts with **1** under the conditions used in this work.

Comparison of the catalytic behavior of **1** with other metallocorroles reveals some striking differences (Table 1). The turnover frequency (TOF) for the **1**/PFIB-catalyzed oxidation of styrene is significantly higher than those seen for the other corrole catalysts (tpfc)$Fe^{IV}Cl$, (tpfc)Mn^{III}, (Br_8tpfc)Mn^{III} or (F_8tpfc)Mn^{III} (tpfc = tris(pentafluorophenyl)corrolato), but the selectivity for production of epoxide by **1**/PFIB is less than the metallocorroles. A comparison of the unsubstituted Mn corrole versus its halogenated analogs ((Br_8tpfc)Mn^{III} and (F_8tpfc)Mn^{III}) reveals the same trend; the halogenated complexes exhibit much higher TOFs with a concomitant loss in selectivity. Chang and co-workers have suggested that halogenation of the corrole ring increases the electrophilicity of the putative high-valent Mn=O intermediate, thereby inducing the large increase in reaction rates.[30] The rate enhancement seen for **1** can be explained in the same way; the corrolazine ring is electron-deficient compared to the corrole ring, and thus the electrophilicity of a high-valent iron−oxo corrolazine intermediate is likely enhanced over the corresponding iron corrole. The electron-withdrawing effect of the corrolazine ligand has been established previously by the comparison of redox potentials for copper−corrolazine/corrole complexes.[31]

The highly active porphyrin catalyst (F_{20}TPP)FeCl was also examined for comparison with **1** (Table 1). Both complex **1** and (F_{20}TPP)FeCl exhibit similar reaction times, although complex **1** decomposes during the course of these reactions, whereas (F_{20}TTP)FeCl remains intact. In the case of styrene, better selectivity for epoxide (68:31, epox/ald) is seen for (F_{20}TPP)FeCl. However, when cyclohexene is employed as substrate, complex **1** matches the performance of (F_{20}TTP)FeCl with respect to reaction time, selectivity for epoxide, and yield. Although the TOFs for (F_{20}TTP)FeCl and **1** given in Table 1 are also comparable, these numbers are lower limits and give only a rough estimate of the inherent reactivity of the two

Scheme 4

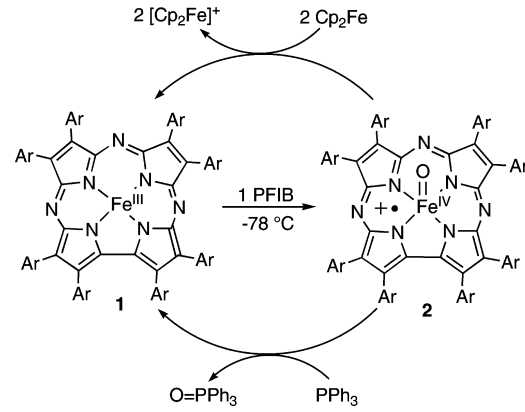

catalysts. However, it is clear from the data that the TON and selectivity for **1** is on par with (F_{20}TTP)FeCl under our conditions.

The observed catalytic activity of **1**/PFIB strongly implicates a high-valent iron−oxo species as the active oxidant. In addition, there is a rapid color change during these catalytic reactions, where dark green **1** converts to a transient dark brown species. This color change is also consistent with the formation of a (Cz)Fe=O intermediate. In contrast, no color change was observed for the reactions with H_2O_2. Taken together these results clearly show that the nature of the oxidant (PFIB vs H_2O_2) is critical in determining the outcome of these reactions. Dramatic differences for H_2O_2 versus PhIO were also noted by Gross and co-workers in reactions with an Mn corrole-albumin conjugate, including the observation of a distinct color change (Mn^{III} to Mn^{V}-oxo) for PhIO, but not for H_2O_2. These workers also concluded that different reactive intermediates were responsible for catalytic oxygen-atom-transfer depending on whether H_2O_2 or PhIO was employed as the sacrifical oxidant.[22]

Low-Temperature UV−Vis Studies. The transient dark brown compound that forms during the catalytic reactions is an obvious candidate for the putative Fe=O intermediate, and efforts were made to trap and characterize this species under single-turnover-like conditions. Addition of one equivalent of PFIB to (TBP$_8$Cz)Fe^{III} at −78 °C in CH_2Cl_2/CH_3OH (Scheme 4) leads to the slow isosbestic conversion of dark green **1** (λ_{max} = 440, 611, 747 nm) to a dark-brown species (**2**) (λ_{max} = 396, 732, 843 nm) (Figure 1).

This new species is stable for many hours at −78 °C, but converts back to **1** upon warming to room temperature (94%

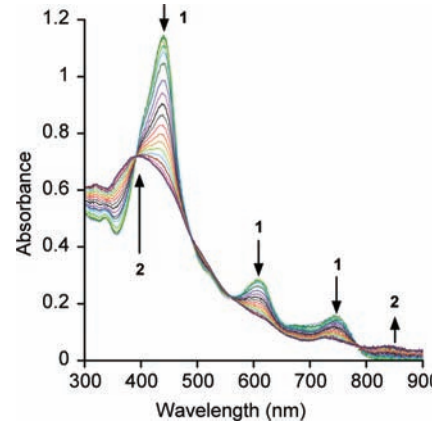

Figure 1. UV−vis spectral changes for the reaction of **1** + PFIB (1 equiv) in CH_2Cl_2/CH_3OH at −78 °C.

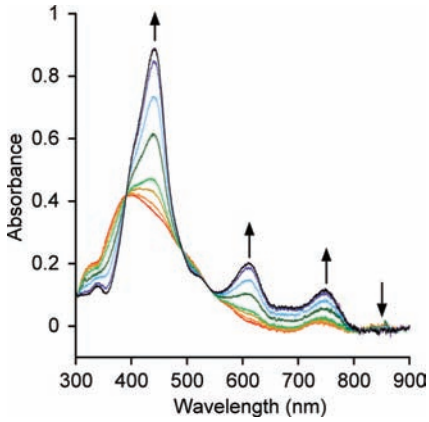

Figure 2. UV−vis spectral change after the sequential addition of Cp_2Fe (0.25 equiv per addition in 25 μL of CH_2Cl_2) to a solution of **2** in CH_2Cl_2/CH_3OH at −78 °C.

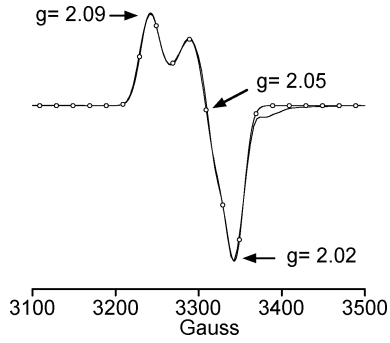

Figure 3. X-band EPR spectrum of **2** in CH_2Cl_2/CH_3OH (3:1) at 15 K. Experimental conditions: frequency, 9.469 GHz; microwave power, 63.62 μW; modulation frequency, 100.00 kHz; modulation amplitude, 10.0 G; receiver gain, 5.02×10^3. Dotted line = simulation.

of **1** recovered). Addition of ferrocene, a one-electron reducing agent, at −78 °C causes the rapid conversion of **2** back to the iron(III) starting material. Sequential addition of aliquots of Cp_2Fe shows that 1.75−2.00 equiv of Cp_2Fe are needed to quantitatively restore the spectrum of **1** (88%), as seen in Figure 2. This titration indicates that **2** is oxidized by two electrons above the $(Cz)Fe^{III}$ state, as expected upon oxygen-atom-transfer from PFIB to **1**. Thus the low-temperature UV−vis data are consistent with the assignment of **2** as a high-valent iron−oxo complex, which can be formulated as $(Cz)Fe^{V}(O)$, or alternatively, with a positive charge distributed on the corrolazine as a π-cation-radical, $(Cz^{+\bullet})Fe^{IV}(O)$. This latter species is equivalent to the familiar "Compound I" intermediate of heme enzymes and their analogous porphyrin model complexes.

EPR Spectroscopy. To obtain more information regarding the electronic configuration of **2**, EPR measurements were performed. The EPR spectrum of **2** at 15 K in CH_2Cl_2/CH_3OH is shown in Figure 3. This spectrum is characterized by $g = 2.09$, 2.05, 2.02, which is distinct from either the intermediate-spin Fe^{III} ($S = {}^3/_2$, $g = 4.0$, 2.0) spectrum seen for **1** in the absence of strong axial donors, or the low-spin Fe^{III} ($S = {}^1/_2$, $g = 2.39$, 2.20, 1.90) spectrum observed for **1** in the presence of pyridine.[18] The spectrum for **2** differs from that of the typical $(Fe^{IV}(O)$(porphyrin π-cation-radical), such as that seen for $[(TMP^{+\bullet})Fe^{IV}(O)]^+$ (TMP = tetramesitylporphyrinato) with $g = 4.36$, 3.58, 1.99. This porphyrin spectrum is assigned to a $S = {}^3/_2$ ground state that arises from ferromagnetic coupling between the Fe^{IV} ion ($S = 1$) and the π-cation-radical.[34] In the heme enzyme horseradish peroxidase, the analogous Compound I species exhibits an EPR spectrum with a broad signal around $g \approx 2.0$ indicative of very weak coupling,[35] which is also quite different from the spectrum seen for **2**. The spectrum for **2** is also distinct from that observed for the recently characterized nonheme $Fe^{V}(O)$ complex, with $g = 1.99$, 1.97, 1.74,[36] one of the few examples of a bona fide Fe^{V}-oxo species.

Interestingly, the spectrum in Figure 3 bears a strong resemblance to that reported for the corrole iron(IV) π-cation-radical complexes $[Fe^{IV}(OEC)Cl]^+$ (OEC = octaethylcorrolato,) and $[Fe^{IV}(OEC)(C_6H_5)]^+$.[37] These complexes exhibit rhombic EPR spectra with $g = 2.12$, 2.07, 2.02 for $[Fe^{IV}(OEC)Cl]^+$ and $g = 2.17$, 2.04, 2.01 for $[Fe^{IV}(OEC)(C_6H_5)]^+$. Both complexes are stable at room temperature, and have been characterized by UV−vis, spectroelectrochemistry, Mössbauer spectroscopy, and in the case of the sigma-bonded phenyl complex, magnetic susceptibility and X-ray crystallography. Thus there is no doubt regarding the structural assignments and electronic configurations of these complexes, and they provide good benchmark data for corrole-based iron(IV) π-cation-radical species. Unlike the former porphyrin complexes, both corrole complexes exhibit *antiferromagnetic* coupling between the Fe^{IV} ($S = 1$) and π-cation-radical spins, giving rise to $S = {}^1/_2$ ground states. Based on this precedent, the EPR spectrum of **2** is assigned as arising from antiferromagnetic coupling between an Fe^{IV} ion and the corrolazine π-cation radical.

To support the assignment of the EPR spectrum for **2**, the effective g values, $g_\perp$ and $g_\parallel$, for an $S = 1$ and $S = {}^1/_2$ spin coupling system were calculated for different J/D values (Figure 4), where J is the Heisenberg exchange coupling between ferryl iron and corrolazine π-cation radical spins and D is the zero-field splitting parameter for ferryl iron ion.[34] The g values of the ferryl iron were taken to be $g_\perp = 2.20$ and $g_\parallel = 2.01$, and an isotropic g value ($g = 2.00$) was used for the corrolazine π-cation radical.[38] The observed EPR g values for **2** can be reproduced with a strong antiferromagnetic interaction, $J/D \approx -1.8$ or very weak interaction, $J/D \approx 0$, as seen in Figure 4. For comparison, the g values for $[(TMP^{+\bullet})Fe^{IV}(O)]^+$ are marked in Figure 4, corresponding to relatively strong ferromagnetic coupling ($J/D \approx 1.5$). The difference in the spin coupling between the corrolazine and porphyrin complexes can be explained by the orbital symmetry of corrolazine and porphyrin π-cation radical spins. As shown with various spectroscopic methods, the porphyrin π-cation radical spin of $[(TMP^{+\bullet})Fe^{IV}(O)]^+$ occupies the a_{2u} orbital, which is not of the proper symmetry to interact with the d_{xz} and d_{yz} orbitals (e_g symmetry), in which the d-electron spins of the ferryl iron are present, if the porphyrin ring is planar. Hence the metal and porphyrin unpaired electrons are either not coupled at all, or else are ferromagnetically coupled. The large spin density on the pyrrole nitrogen atoms in the a_{2u} orbital favors a ground

(34) Fujii, H.; Yoshimura, T.; Kamada, H. *Inorg. Chem.* **1996**, *35*, 2373–2377.
(35) Schulz, C. E.; Rutter, R.; Sage, J. T.; Debrunner, P. G.; Hager, L. P. *Biochemistry* **1984**, *23*, 4743–4754.
(36) de Oliveira, F. T.; Chanda, A.; Banerjee, D.; Shan, X. P.; Mondal, S.; Que, L., Jr.; Bominaar, E. L.; Münck, E.; Collins, T. J. *Science* **2007**, *315*, 835–838.
(37) Van Caemelbecke, E.; Will, S.; Autret, M.; Adamian, V. A.; Lex, J.; Gisselbrecht, J.-P.; Gross, M.; Vögel, E.; Kadish, K. M. *Inorg. Chem.* **1996**, *35*, 184–192.
(38) Oosterhuis, W. T.; Lang, G. *J. Chem. Phys.* **1973**, *58*, 4757–4765.

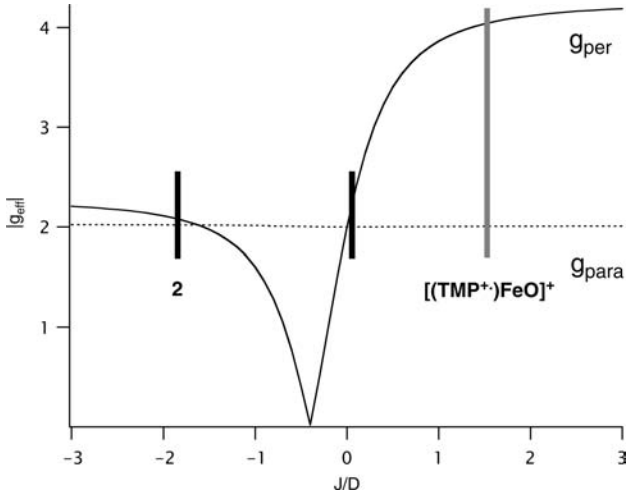

Figure 4. Plot of effective *g* values versus J/D. The solid line shows the g-perpendicular value and the dotted line shows the g-parallel value. The positive and negative signs mean ferromagnetic and antiferromagnetic interactions when the D value is positive. The gray bold line shows the possible J/D value for $[(TMP^{+\bullet})Fe^{IV}(O)]^{+}$ and the black bold lines shows possible J/D values for **2**.

state with a ferromagnetic interaction, as observed.[39] DFT calculations showed that the HOMO of the corrolazine and corrole π-cation radical complexes would be the a_2 and b_1 orbitals, respectively.[40,41] Since the symmetries of the d_{xz} and d_{yz} orbitals are lowered to b_1 and a_2, respectively, upon changing the structure from a porphyrin (D_{4h}) to a corrolazine and corrole (C_{2v}), the spin interactions of the corrolazine and corrole π-cation radical spins with the ferryl iron spin would be symmetry-allowed, leading to ground states with antiferromagnetic interactions for $(Cz^{+\bullet})Fe^{IV}(O)$, $[Fe^{IV}(OEC)Cl]^{+}$ and $[Fe^{IV}(OEC)(C_6H_5)]^{+}$. This analysis corroborates the assignment of **2** as an antiferromagnetically coupled $(Cz^{+\bullet})Fe^{IV}(O)$ complex.

Reactivity of $(TBP_8Cz^{+\bullet})Fe^{IV}(O)$. The UV−vis data, behavior toward reducing agents, and EPR spectroscopy all point to the assignment of the low-temperature species **2** as the high-valent iron−oxo complex $(TBP_8Cz^{+\bullet})Fe^{IV}(O)$. Further confirmation of the identity of **2** came from reactions with oxygen atom acceptors. Reaction of **2** with 1.1 equiv of PPh_3 at −78 °C results in a rapid color change back to the dark green of **1**. Analysis by GC-FID revealed production of $O{=}PPh_3$ in high yield (>99%), and examination of this reaction by UV−vis showed that $(Cz)Fe^{III}$ is quantitatively reformed (data not shown). These results conclusively show that **2** is capable of O-atom transfer, and carries one equivalent of oxygen per iron center.

No reaction is observed when excess cyclohexene is added to **2** at −78 °C, as seen by the lack of any change in the UV−vis spectrum for **2** upon addition of this substrate. However, if **2** is first generated at −78 °C, then warmed to −42 °C and treated with excess cyclohexene, evidence for a reaction is clearly observed. As seen in Figure 5, the addition of excess cyclohexene causes the complete conversion of **2** to the Fe^{III} complex **1** within 30 min. A control experiment shows that the spectrum for **2** is stable for at least 1 h at −42 °C in the absence of cyclohexene. Upon warming a solution of **2** and cyclohexene

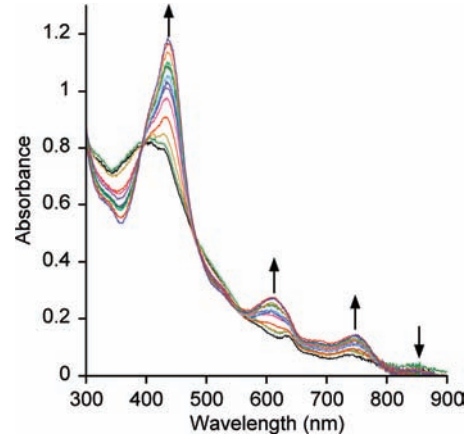

Figure 5. UV−vis spectral changes over 30 min following the addition of cyclohexene to a solution of **2** in CH_2Cl_2/CH_3OH at −42 °C.

at −78 °C directly to room temperature, **2** is converted to **1** (60%), and oxidation products are formed (epox (0%), alcohol (11%), ketone (5%)). The modest combined yield (16%) is not surprising given that **2** likely decays via other competitive pathways upon warming, as evidenced by a 60% recovery of the Fe^{III} complex. However, the absence of epoxide is in contrast to the results from the catalytic oxidation of cyclohexene. This difference may be due to temperature effects; similar changes in product ratios with temperature have been seen for iron−oxo porphyrin-mediated oxidations of alkenes.[39,42,43]

Rapid-Mixing Stopped-Flow UV−Vis Spectroscopy. The reaction between **1** and PFIB at room temperature was monitored by rapid-mixing stopped-flow UV−vis spectroscopy with the goal of spectroscopically characterizing the brown intermediate that forms during the room temperature catalytic reactions. Rapid mixing of **1** with excess PFIB in CH_2Cl_2/CH_3OH results in the time-resolved UV−vis spectra shown in Figures 6 and 7. The data clearly separate into two kinetic phases that are distinguishable by isosbestic conversion in the first phase, followed by the loss of isosbestic behavior in the second. As seen in Figure 6, the initial (0−454 ms) isosbestic conversion involves a decrease and shift of the Soret band for **1** from 435 to 416 nm, along with a loss of the Q-band at 611 nm. The final spectrum at 454 ms strongly resembles that of the low-temperature species **2** seen in Figure 1, in addition to a minor contribution from a small amount of remaining iron(III) complex. The tight isosbestic behavior observed in Figure 6, and in particular the isosbestic point at 389 nm, matches that seen for the low-temperature conversion of **1** to **2** (isosbestic point = 391 nm) in Figure 1. We conclude that the intermediate being formed at room temperature in the first phase of the stopped-flow reaction is the same species as the iron−oxo complex **2** generated at −78 °C.

The second phase of the reaction is shown in Figure 7. There is a loss of the isosbestic point at 389 nm accompanied with a decay of the broad peak at 416 nm, giving a final spectrum with a shoulder at 394 nm. These data correspond to the decay of the iron−oxo species **2**, which ultimately results in corrolazine ring degradation as evidenced by the loss of well-denfiend $\pi-\pi^*$ transitions (Soret and Q bands).

The decay kinetics for the first phase is shown in the inset of Figure 6. The decay of the iron(III) complex was monitored at

(39) Takahashi, A.; Kurahashi, T.; Fujii, H. *Inorg. Chem.* **2009**, *48*, 2614–2625.
(40) Steene, E.; Wondimagegn, T.; Ghosh, A. *J. Phys. Chem. B* **2001**, *105*, 11406–11413.
(41) Tangen, E.; Ghosh, A. *J. Am. Chem. Soc.* **2002**, *124*, 8117–8121.
(42) Gross, Z.; Nimri, S. *J. Am. Chem. Soc.* **1995**, *117*, 8021–8022.
(43) Song, W. J.; Ryu, Y. O.; Song, R.; Nam, W. *J. Biol. Inorg. Chem.* **2005**, *10*, 294–304.

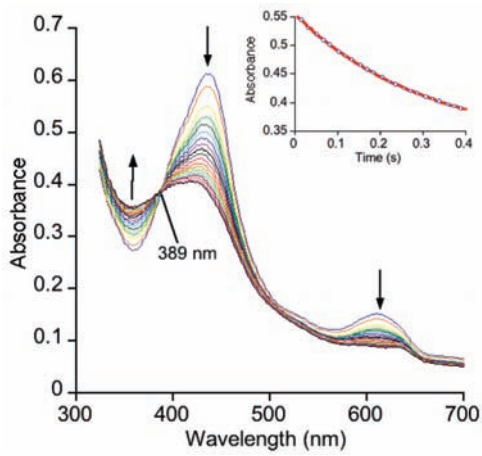

Figure 6. Time-resolved, stopped-flow UV−visible spectra for the reaction of $(TBP_8Cz)Fe^{III}$ (**1**) and PFIB over 454 ms (first phase). Experimental conditions: [**1**] = 2.03×10^{-5} M, [PFIB] = 2.03×10^{-3} M in CH_2Cl_2/CH_3OH (1:1 v:v) at room temperature. (Inset) Plot of absorbance at 435 nm vs time showing the decay of **1** (blue open circles), and the best fit of the data (red line).

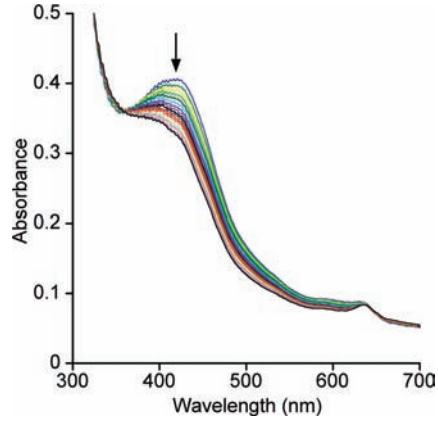

Figure 7. Time-resolved, stopped-flow UV−visible spectra for the reaction of $(TBP_8Cz)Fe^{III}$ (**1**) and PFIB from 0.45−1.5 s (second phase). Experimental conditions: [**1**] = 2.03×10^{-5} M, [PFIB] = 2.03×10^{-3} M in CH_2Cl_2/CH_3OH (1:1 v:v) at room temperature.

435 nm and fit well to a single exponential function, indicative of pseudo-first-order behavior. The best fit gave an observed rate constant of $k_{obs} = 3.19 \pm 0.04$ s^{-1} with [PFIB] = 2.0×10^{-3} M. The k_{obs} values exhibit a linear dependence on the concentration of [PFIB] as shown Figure 8, and the slope of the best-fit line gives an apparent second-order rate constant of $k^1 = 1252$ M^{-1} s^{-1}. The second-order rate constant (k^1) is similar in magnitude to the rate constants reported previously for catalytic epoxidations involving iron(III) porphyrins and PFIB ($k = 10^3 - 10^4$ M^{-1} s^{-1}).[29] These rate constants correspond to the formation of an iron−oxo porphyrin intermediate, which is the slow (i.e., rate-determining) step in the catalytic cycle, and are thus directly comparable to k^1 in Scheme 5.

The stopped-flow data are consistent with the simple two-step mechanism shown in Scheme 5. The first step (k^1) involves the oxidation of **1** by PFIB to give the iron−oxo species **2**, and the rate of this step is linearly dependent on [PFIB], as expected. Here we show PFIB in its solvated form in the presence of methanol. This step may include a pre-equilibrium process involving the coordination of the oxidant to the iron(III) complex as proposed for analogous oxidation processes with iron porphyrins,[27] but we did not observe saturation behavior under

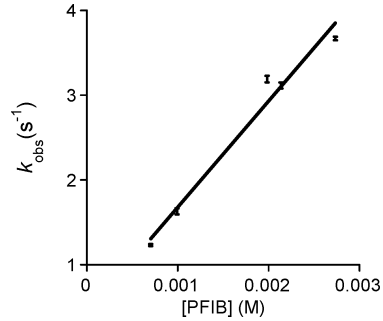

Figure 8. Dependence of k_{obs} on the concentration of the oxidant ([PFIB]) for the reaction of **1** and PFIB, together with the best-fit line. The slope of the best-fit line equals the apparent second-order rate constant (k^1). Experimental conditions: [**1**] = 2.03×10^{-5} M, [PFIB] = 7.03×10^{-4} M − 2.74×10^{-3} M.

Scheme 5

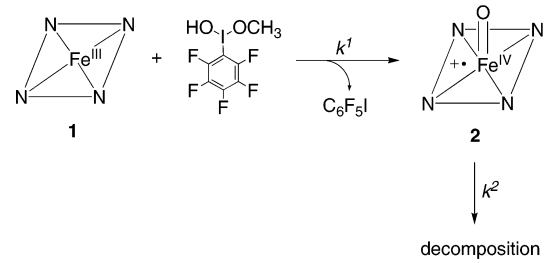

the concentration range of [PFIB] employed. Assuming this equilibrium is present, the apparent second-order rate constant k^1 is actually a composite of the equilibrium constant and the first-order rate constant for conversion of the coordinated oxidant into the iron−oxo complex. The second step in Scheme 5 involves the decomposition of **2** to unidentified products with likely degradation of the corrolazine macrocycle. The kinetics of this step (data not shown) does not fit well to a single exponential function for all [PFIB], although the rate of this step appears to roughly increase with increasing [PFIB]. Multiple decomposition pathways for **2** are likely, including possible reaction with excess PFIB. The analogous Fe^{IV}-oxo porphyrin cation radicals have been shown to react with excess PhIO, leading to the formation of $PhIO_2$ as well as decomposition of the porphyrin complex.[27,44] In addition, if the low-temperature (−78 °C) reaction between **1** and PFIB is run with an excess of PFIB instead of one equivalent, we observe both the rapid formation and decomposition of **2**. This observation is consistent with the general kinetic scheme obtained from the stopped-flow experiments.

Summary and Conclusions

The iron(III) corrolazine is an active catalyst for a variety of oxidation reactions. The nature and scope of these reactions are highly dependent on the nature of the oxidant. When H_2O_2 is used as the external oxidant with **1** as catalyst, thioether substrates can be rapidly and selectively oxidized to sulfoxide. However, **1**/H_2O_2 cannot oxidize alkenes. Changing the oxidant to PFIB dramatically changes the catalytic activity of **1**, and a variety of alkene substrates are easily oxidized. These observations indicate that a different mechanism is operative for the PFIB reactions, the most obvious choice being a mechanism involving a high-valent iron−oxo intermediate as the active

(44) Nappa, M. J.; Tolman, C. A. *Inorg. Chem.* **1985**, *24*, 4711–4719.

oxidant, as opposed to the coordinated hydroperoxo adduct postulated previously for the H_2O_2-dependent reactions. A comparison of the catalytic behavior of **1** with other metallocorroles reveals that the presence of *meso*-N atoms in the corrole ring has a strong influence on catalytic behavior, which can be attributed to an increase in the electrophilicity of the key, high-valent iron−oxo intermediate. With cyclohexene as substrate, complex **1** exhibits comparable turnovers and selectivity for epoxide as found for one of the best porphyrin catalysts ($(TPPF_{20})$FeCl) under identical reaction conditions. These results indicate that metallocorrolazines hold significant promise as catalysts for other oxidation reactions. The direct spectroscopic observation (UV−vis, EPR) of a high-valent iron−oxo corrolazine, **2**, was accomplished by the low-temperature (−78 °C) reaction of PFIB and **1**. The EPR spectrum for **2** is assigned as an antiferromagnetically coupled $Fe^{IV}(O)$ π-cation-radical complex. Although antiferromagnetic coupling is unusual for $Fe^{IV}(O)$ π-cation-radical porphyrins, well characterized Fe^{IV} corrole π-cation-radical complexes, where the axial ligand is not an oxo, are clearly antiferromagnetically coupled. Reactivity studies of **2** with a one-electron transfer agent at low-temperature are consistent with a formal oxidation state for **2** that is two levels above the Fe^{III} state. Reaction with PPh_3 at −78 °C reveals **2** to be a competent oxo transfer agent, helping to confirm its identity as a terminal oxo complex. The necessity to work at low-temperature to stabilize **2** contrasts our previous studies with the analogous Mn^{V}-oxo complex, which was found to be isolable at room temperature.[20] The factors that control the thermal stability of these high-valent metal-oxo complexes remain to be determined. Direct evidence that the low-temperature complex **2** is generated under catalytic conditions at room temperature comes from stopped-flow measurements, which show the rapid isosbestic conversion of **1** to **2**, followed by decomposition of the iron−oxo species. Previously, DFT calculations have suggested that the corrolazine ligand should stabilize the Fe^{V}−oxo configuration over the Fe^{IV}−oxo π-cation-radical.[45] Although our findings indicate the latter configuration applies to **2**, the attainment of an Fe^{V}−oxo complex may still be possible, either by modification of the Cz ligand or the addition of appropriate axial ligands.

Acknowledgment. We thank the NSF (CHE0606614) for financial support. W.D.K. is grateful for a Camille and Henry Dreyfus Environmental Chemistry Postdoctoral Fellowship. H.F. thanks the JST (CREST) and Global COE program. We thank Dr. Angela Wilks for the use of the stopped-flow UV–vis instrument.

JA809183Z

(45) Wasbotten, I.; Ghosh, A. *Inorg. Chem.* **2006**, *45*, 4910–4913.